inorganics

MDPI

Article

Structural, Quantum Chemical, and Cytotoxicity Analysis of Acetylplatinum(II) Complexes with $PASO_2$ and DAPTA Ligands

Stefan Richter [1,†], Dušan Dimić [2,†], Milena R. Kaluđerović [3], Fabian Mohr [4] and Goran N. Kaluđerović [5,*]

[1] Institut für Chemie, Martin-Luther-Universität Halle-Wittenberg, Kurt-Mothes-Straße 2, 06120 Halle, Germany; richter.ste@arcor.de
[2] Faculty of Physical Chemistry, University of Belgrade, Studentski Trg 12–16, 11000 Belgrade, Serbia; ddimic@ffh.bg.ac.rs
[3] Department of Oral, Maxillary, Facial and Reconstructive Plastic Surgery, University Hospital of Leipzig, 04103 Leipzig, Germany; milena.kaluderovic@uniklinik-leipzig.de
[4] Anorganische Chemie, Fakultät für Mathematik und Naturwissenschaften, Bergische Universität Wuppertal, 42119 Wuppertal, Germany; fmohr@uni-wuppertal.de
[5] Department of Engineering and Natural Sciences, University of Applied Sciences Merseburg, Eberhard-Leibnitz-Straße 2, 06217 Merseburg, Germany
* Correspondence: goran.kaluderovic@hs-merseburg.de
† These authors contributed equally to this work.

Abstract

The development of novel platinum-based anticancer agents remains a critical objective in medicinal inorganic chemistry, particularly in light of resistance and toxicity limitations associated with cisplatin. In this study, the synthesis, structural characterization, quantum chemical analysis, and cytotoxic evaluation of four new acetylplatinum(II) complexes (*cis*-[Pt(COMe)$_2$(PASO$_2$)$_2$], *cis*-[Pt(COMe)$_2$(DAPTA)$_2$], *trans*-[Pt(COMe)Cl(DAPTA)$_2$], and *trans*-[Pt(COMe)Cl(PASO$_2$)]: **1–4**, respectively) bearing cage phosphine ligands $PASO_2$ (2-thia-1,3,5-triaza-phosphaadamantane 2,2-dioxide) and DAPTA (3,7-diacetyl-1,3,7-triaza-5-phosphabicyclo[3.3.1]nonane) are presented. The coordination geometries and NMR spectral features of the *cis*/*trans* isomers were elucidated through multinuclear NMR and DFT calculations at the B3LYP/6-311++G(d,p)/LanL2DZ level, with strong agreement between experimental and theoretical data. Quantum Theory of Atoms in Molecules (QTAIM) analysis was applied to investigate bonding interactions and assess the covalent character of Pt–ligand bonds. Cytotoxicity was evaluated against five human cancer cell lines. The $PASO_2$-containing complex in *cis*-configuration, **1**, demonstrated superior activity against thyroid (8505C) and head and neck (A253) cancer cells, with potency surpassing that of cisplatin. The DAPTA complex **2** showed enhanced activity toward ovarian (A2780) cancer cells. These findings highlight the influence of ligand structure and isomerism on biological activity, supporting the rational design of phosphine-based Pt(II) anticancer drugs.

Keywords: platinum(II) complexes; DFT; QTAIM; cytotoxic activity; NMR

Academic Editors: Ana Maria Da Costa Ferreira and João Honorato de Araujo-Neto

Received: 27 June 2025
Revised: 18 July 2025
Accepted: 24 July 2025
Published: 27 July 2025

Citation: Richter, S.; Dimić, D.; Kaluđerović, M.R.; Mohr, F.; Kaluđerović, G.N. Structural, Quantum Chemical, and Cytotoxicity Analysis of Acetylplatinum(II) Complexes with $PASO_2$ and DAPTA Ligands. *Inorganics* **2025**, *13*, 253. https://doi.org/10.3390/inorganics13080253

1. Introduction

Cisplatin has served as the "gold standard" in cancer therapy for more than six decades [1–4]. Although it has been highly effective in treating a wide range of malignancies, its clinical use is hindered by significant drawbacks, including the emergence of drug resistance and severe toxicities affecting the kidneys, auditory system, and central nervous system [5,6]. Alongside cisplatin, other platinum-based chemotherapeutics, such

as carboplatin and oxaliplatin, have also been extensively employed in oncology. However, their therapeutic application is limited by adverse side effects, prompting the exploration of transition metal complexes as alternative anticancer agents [7,8]. The incorporation of metals other than platinum in drug design offers the potential to engage different cellular targets and activate distinct biochemical pathways. Accordingly, compounds containing metals such as titanium, ruthenium, tin, palladium, and gold have emerged as promising candidates in the development of new anticancer therapeutics [9–13].

Although phosphine ligands have traditionally been avoided in biological applications due to their high reactivity and potential oxidative instability, it has been shown that some water-soluble cage phosphines can circumvent these issues and enable the synthesis of kinetically stable, air- and moisture-tolerant Pt(II) complexes [14–16]. In particular, cage phosphines such as PTA, $PASO_2$, and DAPTA exhibit favorable steric protection [17]. These properties, combined with their modularity and solubility profiles, have revitalized interest in phosphine-based Pd(II), Pt(II), Ru(II), and Cu(I) complexes for anticancer applications [18–20]. Several such complexes have demonstrated potent cytotoxic activity against both cisplatin-sensitive and -resistant cancer cells, providing a strong rationale for their continued development [17].

Water-soluble phosphine ligands such as PTA (Figure 1) represent a promising strategy for obtaining water-soluble Pt(II) complexes [17,21–24]. PTA-based Pt(II) compounds are valued for their air and water stability, strong basicity, and compact steric profile. PTA coordinates via the phosphorus atom, forming well-defined square planar geometries and enabling the synthesis of *cis*- and *trans*-isomers in high yields. Their high solubility in water is advantageous for catalytic and medicinal applications. In recent years, various PTA-containing transition metal complexes have been synthesized, including $[Ni(CN)_2(PTA)_3]$, $[PdCl_2(PTA)_2]$, $[PtCl_2(PTA)_2]$, and $[RhCl_2(PTA)_4]$ [11–18,25,26]. Most of these show excellent solubility in polar protic solvents, making PTA an attractive ligand for developing water-soluble cytotoxic drugs. The structurally related ligand $PASO_2$ (2-thia-1,3,5-triaza-phosphaadamantane 2,2-dioxide, Figure 1) differs from PTA by the substitution of a $-CH_2-$ unit with a $-SO_2-$ group, significantly reducing its water solubility [27]. While PTA forms water-soluble complexes, $PASO_2$ counterpair complexes are largely insoluble, limiting its use in aqueous media. Interestingly, both PTA and $PASO_2$ exhibit alkylation behavior at the phosphorus center, although PTA shows competing methylation at nitrogen. Despite structural differences, comparative studies have shown that $PASO_2$ and PTA possess electronically similar donor properties toward metal centers. The water-soluble phosphine ligand 3,7-diacetyl-1,3,7-triaza-5-phosphabicyclo[3.3.1]nonane (DAPTA), shown in Figure 1, has been incorporated into a variety of organometallic complexes, demonstrating both structural versatility and biological relevance. Dicationic digold(II) $[Au_2\{\mu\text{-}(CH_2)_2PPh_2\}_2(DAPTA)_2](OTf)_2$ complexes bearing DAPTA as an ancillary ligand were synthesized and shown to be water-soluble, although their catalytic performance in aqueous media was limited [26]. Modified DAPTA derivatives with chalcogen substitutions (O, S, Se) at the phosphorus center were also prepared and structurally characterized; these species notably enhanced copper-catalyzed azide–alkyne cycloaddition in water, underlining DAPTA's potential in green catalysis [28]. Furthermore, platinum(II) and palladium(II) complexes of DAPTA, *cis*-$[MCl_2(DAPTA)_2]$ and *trans*-$[M(SN)_2(DAPTA)_2]$ (M = Pd(II), Pt(II), SN = *S*-*m*-methylpyrimidine-2-thionate, *S*-4,6-dimethylpyrimidine-2-thionate, *S*-4,6-dihydroxypyrimidine-2-thionate, benzothiazole-2-thionate, benzoxazole-2-thionate, *S*-1,3,4,-thiadiazole-2-thionate, *S*-4,5-*H*-thiazolan-2-thionate, and *S*-pyrimidine-4(1*H*)-one-2-thionate, were prepared [24]. Complexes with DAPTA and with thionate ligands exhibited high cytotoxicity against both cisplatin-sensitive and -resistant ovarian

cancer cells, suggesting DAPTA-based complexes as promising candidates for anticancer drug development.

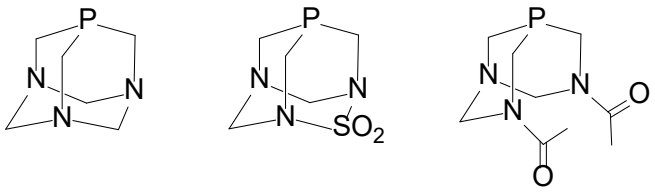

Figure 1. Cage phosphine ligands (from left to right): PTA, $PASO_2$, and DAPTA.

The aim of this contribution is to prepare acetylplatinum(II) complexes with cage phosphine ligands $PASO_2$ and DAPTA: *cis*-[Pt(COMe)$_2$($PASO_2$)$_2$] (**1**), *cis*-[Pt(COMe)$_2$(DAPTA)$_2$] (**2**), *trans*-[Pt(COMe)Cl($PASO_2$)$_2$] (**3**), and *trans*-[Pt(COMe)Cl(DAPTA)$_2$] (**4**). These compounds were characterized by elemental analysis, FTIR spectroscopy, and multinuclear NMR techniques. The structural features of the complexes were evaluated by DFT optimization at the B3LYP/6-311++G(d,p)(C,H,N,O,P,S,Cl)/LanL2DZ(Pt) level of theory, and the calculated bond lengths and angles were compared with experimental data for similar compounds. The ^{1}H and ^{13}C NMR spectra were predicted and analyzed in comparison with experimental spectra. The interactions between the platinum center and donor atoms, as well as non-covalent intramolecular interactions, were examined using the Quantum Theory of Atoms in Molecules (QTAIM). The effects of isomerism and the influence of the chlorido ligand on bonding characteristics were investigated. The cytotoxic activity of complexes **1**, **2**, and **4** was determined against 8505C, A253, A549, A2780, and DLD-1 human cancer cell lines.

2. Results and Discussion

2.1. Synthesis

Complexes **1**–**4** were prepared in the reaction starting from [Pt(COMe)$_2$(NH_2Bn)$_2$] or dinuclear platina-β-diketone [Pt$_2${(COMe)$_2$H}$_2$(μ-Cl)$_2$] according to Scheme 1. The *cis*-configured Pt(II) complex with a $PASO_2$ (**1**) or DAPTA ligand (**2**) showed moderate to good water solubility. The characteristic C=O frequencies of the ligands were observed in the range between 1600 and 1635 cm^{-1}, which is consistent with the literature data [29–31].

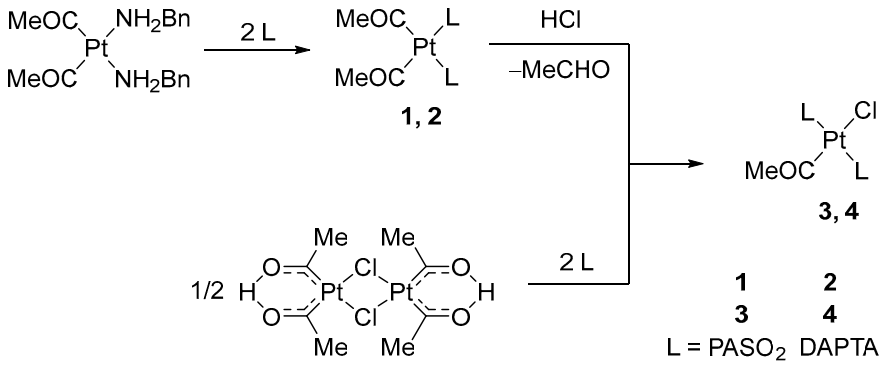

Scheme 1. Synthesis of *cis*- and *trans*-configured acetylplatinum(II) complexes, **1**–**4**.

In the reaction with HCl, complex **1** yielded *trans*-(monoacetyl)platinum(II) complex (Scheme 1). Due to the presence of $PASO_2$ ligands, **1** shows only limited solubility in methanol. After 18 days of reaction time, the mixture was processed to yield **3**, an air-stable, water-insoluble solid in 70% yield. However, the product contained around 20% impurities and could therefore only be characterized by ^{1}H and ^{31}P NMR spectroscopy. Complex **3** is moderately stable in DMSO solution. Initially, clear solutions decompose over time, leading

to browning and the formation of a white precipitate. The reaction of **2** with excess HCl in methanol did not afford the expected compound [Pt(COMe)Cl(DAPTA)$_2$] (**4**). Although the reaction proceeded in a homogeneous phase, ^{31}P NMR analysis of the reaction mixture revealed that decomposition into multiple unidentified phosphorus-containing species occurred within just a few hours.

Given the well-documented reactivity of platinum β-diketonates with various phosphines [32], we investigated the reaction of the dinuclear β-diketonate complex [Pt$_2${(COMe)$_2$H}$_2$(μ-Cl)$_2$] with the cage ligands PASO$_2$ and DAPTA. In a 1:4 molar ratio, reactions proceeded in methanol or dichloromethane, leading to the formation of [Pt(COMe)Cl(PASO$_2$)$_2$] (**3**) and [Pt(COMe)Cl(DAPTA)$_2$] (**4**). PASO$_2$ reacted with [Pt$_2${(COMe)$_2$H}$_2$(μ-Cl)$_2$] selectively in dichloromethane, yielding **3** in a 37% yield. In contrast, DAPTA in reaction with [Pt$_2${(COMe)$_2$H}$_2$(μ-Cl)$_2$] gave **4** in a good yield (85%) when methanol was used. Both products were isolated as white, air-stable, water-insoluble solids via ether precipitation. Notably, **4** could not be obtained through protolytic cleavage, highlighting the importance of this synthetic approach. Complexes **3** and **4** were not soluble in water. Although soluble in DMSO, complex **3** showed limited solution stability. Moreover, complex **3** decomposition and precipitation occurs within hours. This restricted the spectroscopic analysis to ^{1}H and ^{31}P NMR, with only **3** providing a meaningful ^{13}C NMR spectrum. The identity and purity of the products were confirmed by NMR spectroscopy.

2.2. Characterization

The ^{1}H, ^{13}C, and ^{31}P NMR chemical shifts of the compounds **1**–**4** are presented in Table 1. The NMR spectra of *cis*-isomers of complexes with PASO$_2$ and DAPTA are complex (Figure 2, Figure 3 and Figures S1–S4), due to the existence of several groups of hydrogen atoms, according to Figure 2. The protons from the PASO$_2$ on the upper rim appeared as a complex AA′BB′MM′X spin system. Four of these protons can be assigned as an AA′BB′ pattern, while the X component corresponds to the coupling with the ^{31}P nucleus. The two methylene protons on the upper rim are enantiotopic and appear as a single signal, observed as a doublet due to a two-bond coupling with the ^{31}P nucleus. These protons constitute the MM′ part of the spin system. In contrast, the two methylene groups on the lower rim each form separate AB spin systems, characterized by a typical two-bond hydrogen–hydrogen coupling. The ^{1}H NMR spectrum of **2** is given in Figure 3. Hydrogen atoms from the methyl groups of DAPTA and acetyl ligands resonate between 2 and 2.4 ppm. In the case of the acetyl methyl protons, satellites with a typical $^{3}J_{Pt,H}$ coupling of 17.2 Hz could be observed at 2.14 ppm.

Table 1. Selected spectroscopic data of the complexes *cis*-[Pt(COMe)$_2$L$_2$] (**1**, in DMSO-d$_6$, and **2**, in CD$_3$OD; L = PASO$_2$, DAPTA) and *trans*-[Pt(COMe)ClL$_2$] (**3** and **4**, in DMSO-d$_6$) (δ in ppm, *J* in Hz).

	$\delta(P_{\text{not coor.}})$	$\delta(P)$ ($^{1}J_{Pt,P}$)	$\Delta\delta$ [a]	PtCOC*H*$_3$	PC*H*$_2$N	PtCOC*H*$_3$	PtC*O*CH$_3$
				δ_H ($^{3}J_{Pt,H}$)		δ_C ($^{2}J_{Pt,C}$)	δ_C
1	−113.4	−77.3 (1440)	36.1	1.93 (15.9)	3.97 [b]	44.1 (330.2)	242.4
2	−74.1	−42.2 (1496)	32.0	2.13 (17.2)	3.80 [b]	44.4 (280.9)	253.1
3	−113.4	−67.2 (3325)	46.2	2.21 (12.6)	4.13 [b]	48.1	209.3
4	−74.1	−35.0 (3200)	39.1	2.31 (n.o.[c])	3.85 [b]	-	-

[a] $\Delta\delta(P) = \delta(P_{coor.}) - \delta(P_{not\ coor.})$, [b] isolated signal of two protons of the upper rim. [c] Not observed.

In all the studied complexes, the methyl carbon atoms of the acetyl ligands displayed complex signal patterns in the ^{13}C NMR spectra. These patterns arise from an ABM spin system (A, B = ^{31}P; M = ^{13}C) and the presence of satellite signals corresponding to an ABMX

spin system (X = ^{195}Pt). Spectral analysis of complex **1** using the PERCH software (Perch Solutions Ltd, Kuopio, Finland.) confirmed the assignment of an ABX spin system.

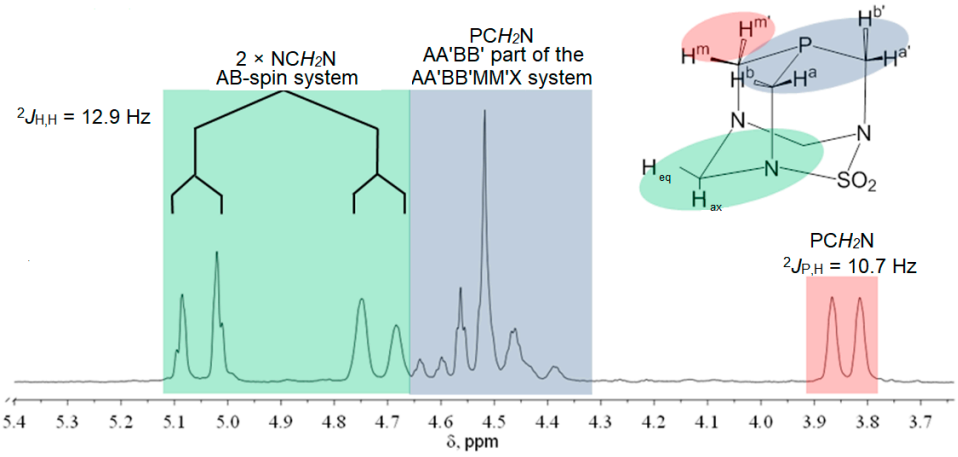

Figure 2. ^{1}H NMR spectrum of $PASO_2$-ligand and spin system (DMSO-d_6, 200 MHz).

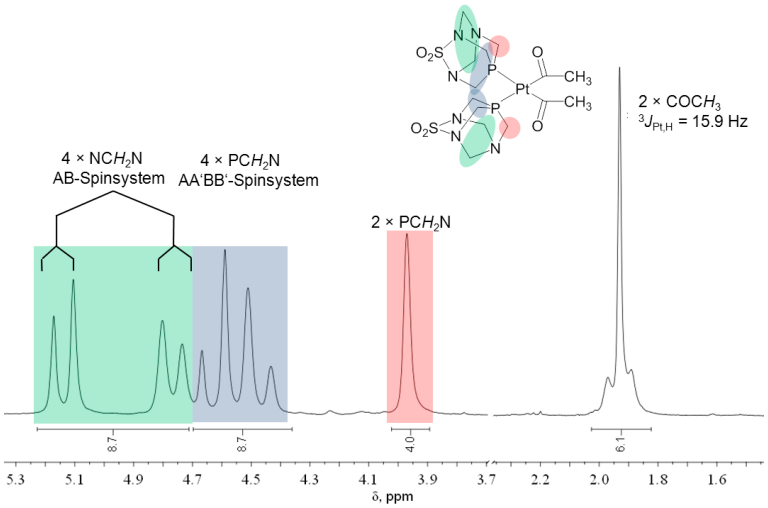

(**a**)

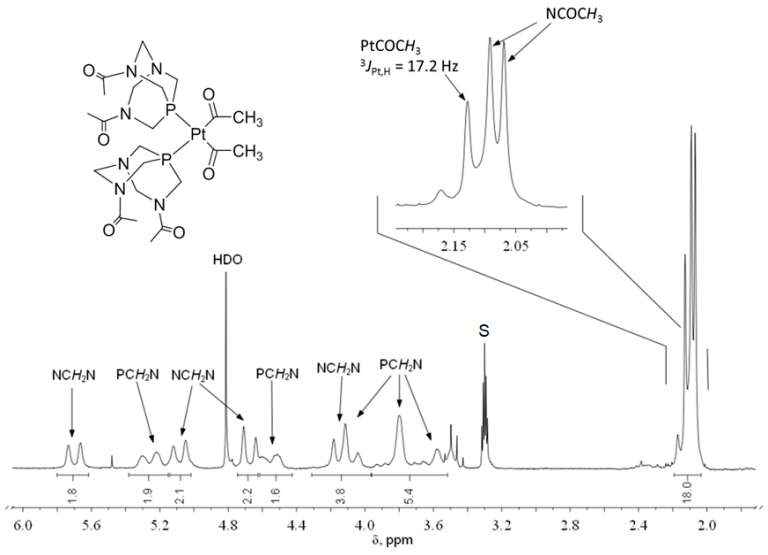

(**b**)

Figure 3. ^{1}H NMR spectrum of (**a**) *cis*-[Pt(COMe)$_2$(PASO$_2$)$_2$], **1** (DMSO-d_6, 200 MHz), and (**b**) *cis*-[Pt(COMe)$_2$(DAPTA)$_2$], **2** (CD_3OD, 200 MHz; S = solvent).

The carbonyl carbon atoms of the acetyl groups in complexes **1** and **2** appeared as multiplets in the ^{13}C NMR spectra, consistent with ABMX spin systems (A, B = ^{31}P; M = ^{13}C; X = ^{195}Pt).

The $^{1}J_{Pt,P}$ coupling constants obtained from the ^{31}P NMR spectra (1440 Hz (**1**) and 1496 Hz (**2**), Table 1) confirm the *cis* configuration of complexes **1** and **2**. For comparison, related compounds such as *cis*-[Pt(COMe)$_2$(PPh$_3$)$_2$] exhibit higher values, ranging from 1563 to 1591 Hz [31]. Notably, the ^{31}P NMR chemical shift in **2** is significantly upfielded (28 ppm) compared to **1**. The resonances observed relative to the corresponding free ligands ($\Delta\delta(P) = \delta(P_{coor.}) - \delta(P_{not\ coor.})$) fall within the range of 32.0–36.1 ppm (Table 1). While the ^{31}P NMR spectra of **1** displays a singlet with accompanying platinum satellites, **2** shows signal splitting both in the main phosphorus resonance and in its platinum satellites, indicating magnetic non-equivalence of the two phosphorus nuclei. This splitting might be attributed to restricted rotation of the *cis*-coordinated DAPTA ligands or to intrinsic asymmetry of the ligand due to the spatial arrangement of its acetyl substituents. The $^{2}J_{P,P}$ coupling constant of 20 Hz is in the typical range for *cis*-coordinated phosphines [33].

The *trans*-bis(phosphane)acetylchloridoplatinum(II) complexes **3** and **4**, both featuring cage phosphines PASO$_2$ and DAPTA, exhibit significantly higher $^{1}J_{Pt,P}$ coupling constants (3036–3317 Hz) compared to their *cis*-diacetylplatinum(II) counterparts (1440–1496 Hz). This substantial increase for about 1700 Hz clearly supports the *trans* configuration of the phosphorus donor atoms. The observed values are also consistent with those reported for related *trans* complexes, such as [Pt(COMe)Cl(PPh$_3$)$_2$] ($^{1}J_{Pt,P}$ of 3470 Hz) [31,34] and *trans*-organoplatinum(II) cage phosphine derivatives, where the $^{1}J_{Pt,P}$ ranges between 2560 and 2720 Hz [35]. On the other hand, acetyl–platinum(II) complexes **3** and **4** showed significantly higher $^{1}J_{Pt,P}$ values (~3300 Hz) thus pointing out to *trans*-coordinated phosphine ligands. This is in accordance with reported values for *trans*-configured complexes, such as *trans*-[Pt(COMe)Cl(PPh$_3$)$_2$] ($^{1}J_{Pt,P}$ of 3470 Hz).

In the ^{1}H NMR spectra, the methyl protons of the acetyl ligands resonate between 2.03 and 2.31 ppm, with similar $^{3}J_{Pt,H}$ coupling values across both **1** and **2**. In the case of **1**, the PASO$_2$ ligands give two separate signals: 4.05 ppm for protons in the upper plane and 4.52 ppm for those in the lower. Interestingly, coordination to the platinum center eliminates the observable proton–phosphorus coupling for the upper-plane protons.

For **2**, only the methyl protons of the DAPTA ligand and the Pt–COCH$_3$ units appear as distinct signal patterns (Figure 3b). Integration assigns 18 protons to these methyl groups, while the remaining 20 protons from the DAPTA framework resonate between 3.5 and 5.8 ppm and were assigned via ^{13}C–^{1}H COSY correlation.

Unlike **2**, complex **1** shows well-resolved upper and lower plane signals in its ^{1}H NMR spectrum (Figure 3a). The four protons of the upper plane form an AA′BB′ spin system appearing as a multiplet between 4.4 and 4.7 ppm. The lower-plane protons form an AB system with four lines, slightly more downfield. Notably, upon coordination to platinum(II), the $^{2}J_{P,H}$ coupling of the PC*H*$_2$N methylene group (3.97 ppm) disappears, resulting in a broad singlet in the ^{1}H NMR spectrum.

The methyl carbon atoms of the acetyl ligands exhibit complex signal patterns in the ^{13}C NMR spectra. These arise from overlapping ABM spin systems (A, B = ^{31}P; M = ^{13}C) along with their corresponding platinum satellites, forming an ABMX spin system (X = ^{195}Pt). For **1** and **2**, spectral analysis of the ABM pattern was successfully performed.

It is well known that DMSO can induce solvolysis of platinum(II) complexes (cisplatin, carboplatin, oxaliplatin), especially those with labile monodentate ligands, leading to the formation of a mixture of solvolyzed species [36]. From our previous studies, on a K[PtCl$_2$(L-pro$_{-H}$)], we have also observed that DMSO-induced ligand substitution processes, under

certain conditions, occur with the formation of a [PtCl(L-pro$_{-H}$)(DMSO)] complex, therefore affecting in vitro activity [37].

To assess stability, we analyzed aged DMSO-d_6 solutions (stored for up to 96 h at room temperature) by ^{31}P NMR spectroscopy (Figure S5). After 96 h of storage, the ^{31}P NMR spectrum revealed traces of a new species, which is most likely a solvolysis product gradually forming in solution.

Stability of complexes **1** and **2** was determined by thermogravimetric analysis. The first step in the decomposition of these compounds was determined at 148 °C (1) and 141 °C (2), yielding a mass loss of 6.6%, which corresponded to the removal of one acetyl group. The second step was observed at 320 (**1**) and 290 °C (**2**). Both of these steps were characterized by an exothermic mass loss. The decomposition to elemental platinum was not complete, even at 1000 °C, with mass reductions of 61.2% and 55.7% for **1** and **2**, respectively.

2.3. Structure Optimization and NMR Spectra Prediction

The optimization of the structures predicted based on the spectroscopic data was performed at the B3LYP/6-311++G(d,p)(C,H,N,O,S,P,Cl)/LanL2DZ(Pt) level of theory in vacuum without any geometrical constraints. This level of theory was suggested in references [38,39] for the optimization of platinum complexes and assignation of spectra. The optimized structures are presented in Figure 4.

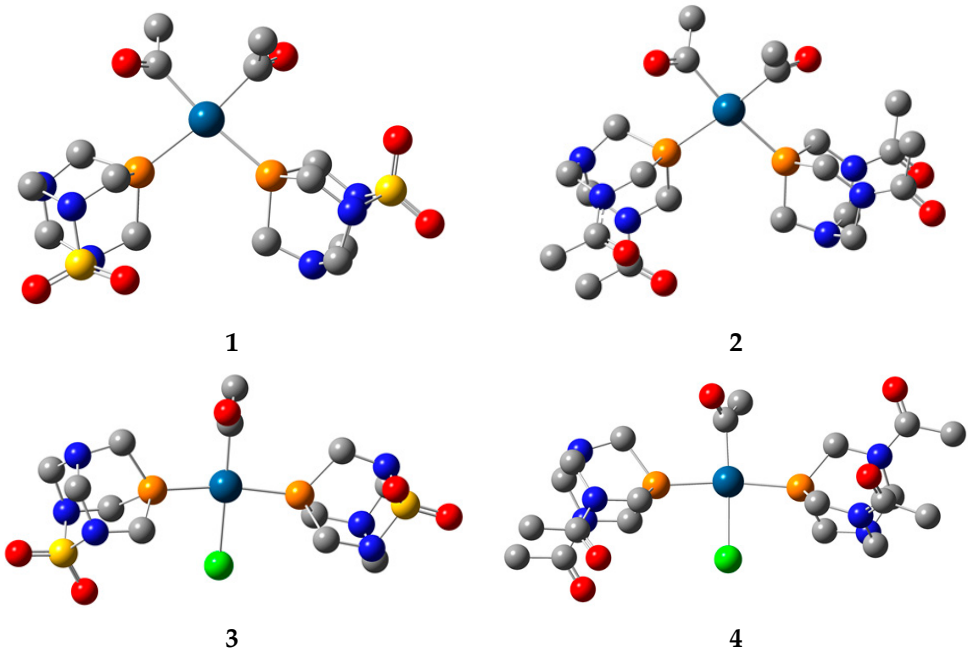

Figure 4. Optimized structures of complexes **1**–**4** at B3LYP/6-311++G(d,p)(C,H,N,O,P,S,Cl)/LanL2DZ(Pt) level of theory (hydrogen atoms are omitted for clarity. Carbon—gray, nitrogen—blue, oxygen—red, sulphur—yellow, phosphorus—dark yellow, chlorine—green, platinum—dark blue).

In the optimized structure of **1**, the ligands are positioned in a square planar geometry. The Pt−P bond distances are 2.422 and 2.426 Å, and they are slightly longer than the two Pt−C bond lengths (2.075 and 2.076 Å). The angle between two PASO2 ligands is 101.1°. The angles enclosed by phosphorus, platinum, and carbon atoms are 86.8 and 85.7°, while two acetyl groups form an 89.4° angle. In the *trans*-isomer, the Pt−P bond distances in complex **3** are 2.337 and 2.329 Å, with the small difference originating from the intramolecular interactions with the chlorido ligand, as explained in the following section. The Pt−P bonds in the *trans*-isomer are shorter, because of the voluminosity of the ligands and the special configuration. The bond lengths between the central metal ion and the carbon and chlorine atoms are 2.023 and 2.521 Å. The angle between two

phosphorus atoms and platinum(II) is 170.0°. The angles enclosed by phosphorus, Pt(II), and carbon are greater (96.1 and 91.8°) than those including the chlorido ligand (87.1 and 84.9°). When complex **2** is examined, the Pt−P distances are 2.437 and 2.419 Å, which is similar to complex **1**, which is to be expected, bearing in mind the geometry of the ligand. The Pt−C bond lengths are almost the same when compared to complex **1** (2.07 Å). The same applies to the P−Pt−P (100.2°), P−Pt−C (86.1 and 84.4°), and C−Pt−C (87.6°) angles. When the trans-isomer with DAPTA ligand is examined, the Pt−P bond lengths (2.336 and 2.346 Å) are shorter than in complex **2**, but comparable to complex **4**. This result also demonstrates that the geometrical parameters depend on the symmetry of the complex and various intramolecular interactions between ligands, as will be explained further. The P−Pt−P angle is 170.1°, while angles that include chlorido ligands and phosphorus atoms are 86.6 and 85.0°.

The geometrical parameters obtained from the DFT-optimized structures are in good agreement with those reported in the literature for similar Pt(II) complexes [21,40]. The calculated Pt–P bond lengths in the *cis*-isomers (2.419–2.437 Å) are slightly longer than those observed experimentally (ca. 2.25–2.29 Å), which is a known trend for B3LYP/LanL2DZ-based calculations. The Pt–C bond lengths in our study (2.07–2.08 Å) align well with experimental values (2.05–2.11 Å), and the calculated P–Pt–P and C–Pt–C angles (ca. 100–101° and 87–89°, respectively) also closely match the experimentally determined distorted square planar geometries. For the *trans*-isomers, the computed P–Pt–P angles (~170°) and Pt–P bond lengths (ca. 2.33–2.35 Å) are consistent with those reported for related *trans*-[Pt(Et)Cl(PTA)$_2$], *trans*-[Pt(C≡CPh)$_2$(PTA)$_2$], *trans*-[PtI$_2$(DAPTA)$_2$], and *trans*-[Pt(C≡CPh)$_2$(PEt$_3$)$_2$] complexes, confirming the validity of the theoretical model in reproducing realistic molecular structures.

The applicability of the selected level of theory for the optimization of the structure was additionally examined by comparison between experimental and theoretical ^{1}H and ^{13}C NMR spectra of complex **2**. This compound was chosen as the experimental peaks were well-resolved in the ^{1}H and ^{13}C NMR spectra. The structure of complex **2** was reoptimized in methanol using a CPCM solvent model. The chemical shifts were calculated by subtracting the chemical shielding of hydrogen/carbon atoms from the chemical shielding of the same atom types in tetramethylsilane (TMS). The two data sets were compared by calculating the correlation coefficient (R^2), the mean absolute error (MAE), root-mean-square deviation (RMSD), slope, and bias, as suggested in references [41,42]. These parameters are listed in Table 2. The MAE parameter is determined as the average absolute difference between experimental and theoretical values.

When experimental and theoretical values for ^{1}H NMR chemical shifts are compared, a high correlation coefficient (0.996) and a low MAE value (0.32 ppm) are obtained. The slope of this dependence was 0.996, which proved that corrections of the theoretical values were not necessary. Additionally, the low RMSD value of 0.38 ppm and bias of 0.13 ppm were in line with this conclusion [41].

On the other side, the correlation coefficient for the ^{13}C NMR chemical shift values was also very high (0.999), but the MAE, RMSD, and bias values indicated the need for slight correction of the values (Table 2). Based on the value of the slope between the theoretical and experimental values (0.971), the correction coefficient was determined. Upon correction, the MAE value lowered to 2.8 ppm, followed by a decrease in RMSD (3.2 ppm) and bias (−0.7) values. This comparison also allows us to conclude that the selected level of theory is appropriate for describing complexes and can be used for a detailed examination of the stabilization interactions in the following section.

Table 2. Experimental and theoretical (at B3LYP/6-311++G(d,p)(H,C,N,O,P)/LanL2DZ(Pt) level of theory) ^{1}H and ^{13}C chemical shifts of complex **2** (in ppm).

^{1}H NMR	Experimental	Theoretical	^{13}C NMR	Experimental	Theoretical	Corrected Theoretical
$NCOCH_3$	2.07	1.94	$NCOCH_3$	21.4	24.1	23.4
$PtCOCH_3$	2.13	1.97	$NCOCH_3$	21.8	24.6	23.9
PCH_2N	3.53	2.91	PCH_2N	40.6	44.3	43.0
PCH_2N	3.8	3.50	PCH_2N	45.4	46.9	45.5
PCH_2N+ NCH_2N	4.12	3.71	$PtCOCH_3$+PCH_2N	44.4	51.4	49.9
PCH_2N	4.55	3.86	NCH_2N	66.9	66.6	64.6
NCH_2N	4.68	4.46	NCH_2N	68.1	71.5	69.4
NCH_2N	5.08	4.70	$NCOCH_3$	171.9	172.3	167.3
PCH_2N	5.26	5.06	$NCOCH_3$	172.2	173.9	168.8
NCH_2N	5.7	5.82	$PtCOCH_3$	253.1	264.7	257.0
R^2		0.996	R^2		0.999	0.999
MAE [ppm]		0.32	MAE [ppm]		3.5	2.8
RMSD [ppm]		0.38	RMSD [ppm]		4.8	3.2
Slope		0.996	Slope		0.971	1.00
Bias [ppm]		0.13	Bias [ppm]		−3.4	−0.7

2.4. QTAIM Analysis

The coordination between donor atoms and central platinum ions was explored through the Quantum Theory of Atoms in Molecules (QTAIM), a reliable framework for evaluating metal–ligand bonding characteristics and estimating interaction energies in platinum-based complexes [43–45]. For key bonding interactions, several descriptors were extracted at the bond critical points (BCPs), including electron density (ρ(r)), the Laplacian of electron density ($\nabla^2\rho(r)$), kinetic energy density (G(r)), potential energy density (V(r)), total energy density (H(r) = G(r) + V(r)), and interatomic bond energy (Ebond = V(r)/2) [43]. According to the classification by Bader and Essen, bonds with ρ(r) > 0.1 a.u. are identified as shared-shell or covalent interactions, whereas those with ρ(r) near 0.01 a.u. correspond to closed-shell interactions, encompassing hydrogen bonding, ionic bonds, or van der Waals forces [46,47]. An expanded interpretation was later introduced by Bianchi et al., using the ratio of G(r) to V(r) to distinguish bonding types: covalent bonds show −G(r)/V(r) < 1; partially covalent (transit) interactions lie between 1 and 2; and interactions with −G(r)/V(r) > 2 are considered predominantly ionic [48]. Another indicator of bond nature is the sign of the total electron energy density—negative values typically suggest a covalent character. The estimation of interatomic interaction energy was based on the method by Espinosa, in which energy is derived from the local potential energy density at the BCP [49]. Table 3 provides an overview of the QTAIM-derived parameters for complexes **1**–**4**. Due to the symmetrical structures of these compounds, only one representative bond per bond type is listed. The BCPs in structures of complexes are shown in Figure 5.

Table 3. The calculated Bond Critical Points (BCPs) properties at the DFT/B3LYP-D3BJ/6-311+G(d,p)(H,C,N,O,P,Cl)/LanL2DZ(Pt) level of theory of complexes **1**–**4**.

Bond	ρ(r) [a.u.]	$\nabla^2\rho(r)$ [a.u.]	G(r) [kJ mol^{-1}]	V(r) [kJ mol^{-1}]	H(r) [kJ mol^{-1}]	−G(r)/V(r)	E_{bond} [kJ mol^{-1}]
			1				
Pt−P	0.082	0.147	166.5	−236.7	−70.2	0.7	−118.3
Pt−C	0.130	0.171	252.5	−392.9	−140.4	0.6	−196.4

Table 3. *Cont.*

Bond	ρ(r) [a.u.]	$\nabla^2\rho(r)$ [a.u.]	G(r) [kJ mol^{-1}]	V(r) [kJ mol^{-1}]	H(r) [kJ mol^{-1}]	−G(r)/V(r)	E_{bond} [kJ mol^{-1}]
O···H	0.010	0.033	18.3	−15.2	3.1	1.2	−7.6
H···H	0.006	0.019	10.1	−7.8	2.3	1.3	−3.9
			2				
Pt−P	0.084	0.150	171.0	−243.7	−72.8	0.7	−121.9
Pt−C	0.131	0.183	260.9	−401.6	−140.7	0.6	−200.8
O···H	0.007	0.022	12.5	−10.8	1.7	1.2	−5.4
H···H	0.006	0.020	10.6	−8.2	2.4	1.3	−4.1
			3				
Pt−P	0.098	0.142	190.4	−287.5	−97.2	0.7	−143.8
Pt−C	0.144	0.168	277.7	−445.3	−167.6	0.6	−222.6
Pt−Cl	0.059	0.163	139.6	−172.3	−32.7	0.8	−86.2
O···H	0.006	0.020	11.2	−9.1	2.1	1.2	−4.6
H···H	0.004	0.134	7.1	−5.4	1.7	1.3	−2.7
H···Cl	0.008	0.025	13.6	−10.6	3.1	1.3	−5.3
			4				
Pt−P	0.098	0.140	187.4	−282.5	−95.2	0.7	−141.3
Pt−C	0.145	0.172	282.0	−451.4	−169.3	0.6	−225.7
Pt−Cl	0.059	0.163	139.6	−172.5	−32.8	0.8	−86.2
O···H	0.007	0.026	14.4	−11.9	2.5	1.2	−6.0
H···H	0.005	0.018	9.6	−7.3	2.3	1.3	−3.6
H···Cl	0.008	0.025	13.3	−10.5	2.9	1.3	−5.2

When the results from Table 3 are examined, it can be concluded that in complex 1, bonds between phosphorus/carbon and platinum have a partially shared-shell character, with electron densities of around 0.1 a.u. Higher values of electron density in Pt−P interactions indicate stronger bonds. This is also reflected in the interatomic energy of −196.4 kJ mol^{-1}, when compared to −118.3 kJ mol^{-1} (Pt−P). Both of these interactions also have a total energy density lower than 1, and a −G(r)/V(r) ratio of 0.7/0.6. Other platinum complexes also contained interactions between the central metal ion and ligands that had small values of electron densities, positive values of Laplacian, and negative values of H(r), which suggested partial covalent characters [38]. Other interactions also influence the overall stability of the complex. The first type of interactions is denoted as O···H, and it is formed between the carbonyl group of the acetyl ligand and $PASO_2$. This interaction is characterized by low electron density (0.010 a.u.), characteristic of closed-shell interactions, with positive H(r) values. The energy of this interaction is −7.6 kJ mol^{-1}. The *cis*-configuration of ligands allows the formation of H···H interactions, with even lower electron density (0.006 a.u.) and energy of −3.9 kJ mol^{-1}. In the *trans*-configured complex (**5**), the value of electron density in Pt−P (0.098 a.u.) and Pt−C (0.144 a.u.) is higher when compared to the *cis*-isomer. The energies of these interactions are significantly higher than those previously discussed. It is important to note that these interactions still have values of the parameters that resemble shared-shell interactions. Besides stronger bonds, the configuration of ligands around the central metal ion influences the formation

of other interactions. Only one O···H interaction is present between the acetyl ligand and PASO2, with energy of −4.6 kJ mol^{-1}. The orientation of the acetyl group also leads to the formation of the H···H with the PASO2 ligand (−2.7 kJ mol^{-1}). The importance of the chlorido ligand is reflected in the electron density of the Pt−Cl bond of 0.059 a.u. and the interaction energy of −86.2 kJ mol^{-1}, which is lower than for the bonds with carbon and phosphorus. An additional weak type interaction exists between the chlorido ligand and the hydrogen atoms of $PASO_2$. This interaction has an energy of −5.3 kJ mol^{-1}. The total energy density of the BCP between chlorine and hydrogen atoms is 3.1 kJ mol^{-1}, while −G(r)/V(r) is 1.3. The significance of the weak interactions for the stability of platinum(II) complexes was also discussed in reference [50].

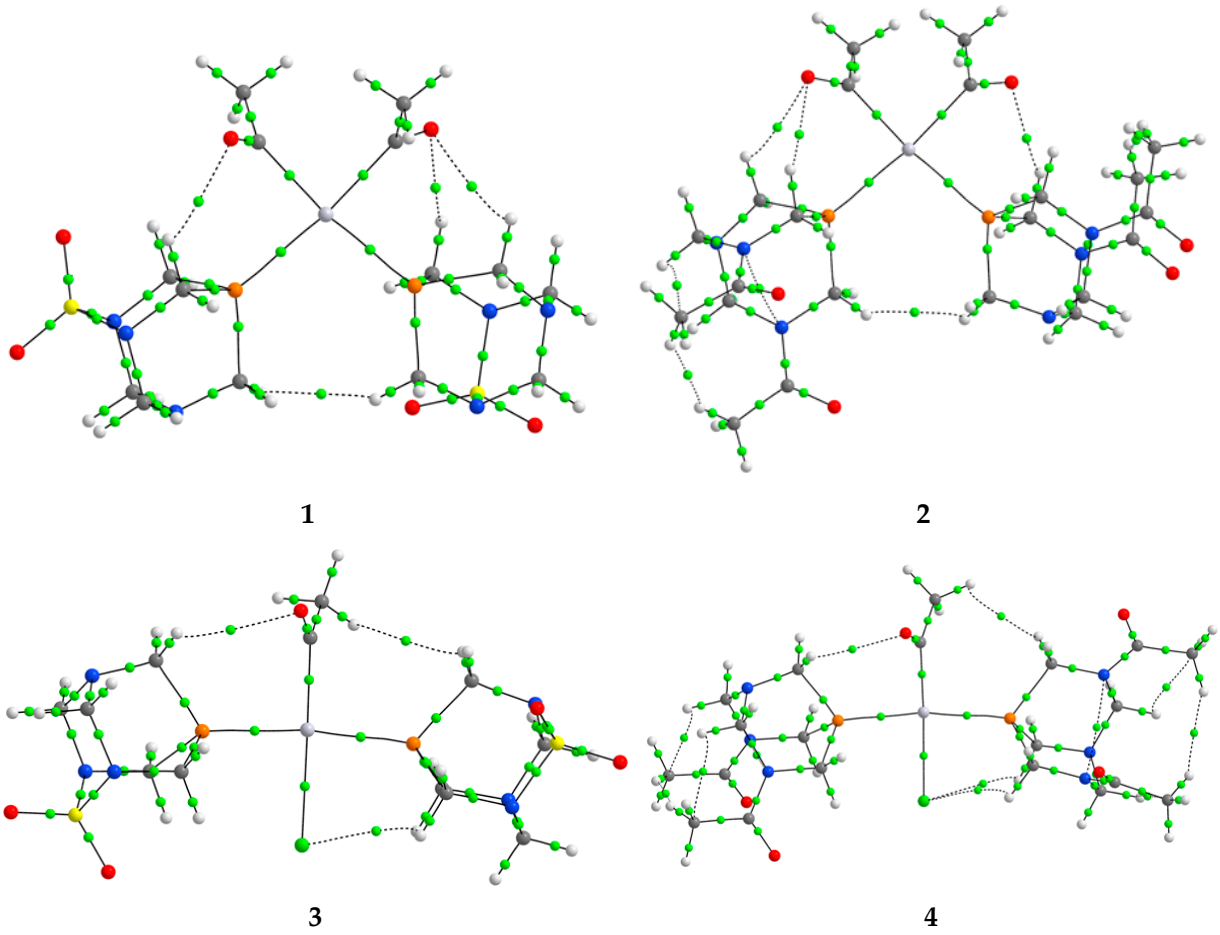

Figure 5. The BCPs (green spheres) in complexes **1**–**4**.

The QTAIM analysis revealed systematically higher electron densities at the bond critical points and more negative interaction energies for Pt–P bonds in *trans*-configured complexes **3** and **4** compared to their *cis* counterparts, **1** and **2**, consistent with stronger metal–ligand interactions. This observation is further supported by the significantly larger $^{1}J_{Pt–P}$ coupling constants recorded for the *trans*-complexes (~3300 Hz) relative to the *cis*-isomers (~1450 Hz), which typically correlate with increased covalency and orbital overlap. Additionally, the Pt–P bond lengths were shorter in the *trans*-complexes, indicating enhanced bond order. Taken together, these data qualitatively suggest a greater extent of π-backdonation or covalent character in the *trans*-isomers. Further studies involving orbital decomposition approaches would be required to rigorously assess the extent of π-backbonding; however, the current results reflect the influence of ligand geometry on electronic structure and bonding strength.

2.5. Cytotoxicity

Four new acetylplatinum(II) complexes were tested against the five human cancer cell lines: 8505C (thyroid cancer), A253 (head and neck tumor), A549 (lung carcinoma), A2780 (ovarian cancer), and DLD-1 (colon carcinoma) (Table 4). For comparison, the cytotoxicity of cisplatin is also included.

Table 4. IC_{50} [μM][a] values of complexes **1**, **2**, and **4** against 8505C (thyroid), A253 (head and neck), A549 (lung), A2780 (ovarian), and DLD-1 (colon carcinoma) [a].

	IC_{50} [μM] ± SD				
Compound	**8505C**	**A253**	**A549**	**A2780**	**DLD-1**
$PASO_2$, DAPTA	>100	>100	>100	>100	>100
1	2.52 ± 0.11	2.33 ± 0.27	1.03 ± 0.18	0.59 ± 0.02	48.85 ± 1.07
2	9.50 ± 0.30	9.64 ± 0.19	10.25 ± 1.13	0.65 ± 0.22	>150
4	57.20 ± 3.14	76.19 ± 3.05	6.56 ± 2.08	1.22 ± 0.29	>150
cisplatin	5.02 ± 0.23	0.81 ± 0.20	1.51 ± 0.02	0.55 ± 0.03	5.14 ± 0.12

[a] Average value ± standard deviation from three experiments.

The free cage phosphines $PASO_2$ and DAPTA exhibited no cytotoxic activity within the tested concentration range (0–100 μM) against the investigated cell lines. Coordination of $PASO_2$ and DAPTA ligands to the platinum center markedly alters tumor cell response. Coordination can influence key properties such as lipophilicity, cellular uptake, and target selectivity, resulting in distinct mechanisms of action compared to the free ligands. These ligands were also selected to enhance solubility and stability in biologically relevant media, further supporting their role in modulating the overall cytotoxic effects. The *cis*-diacetylplatinum(II) complexes **1** and **2** exhibited moderate to high cytotoxicity toward most of the tested cell lines, except DLD-1. Among all the tested compounds, only complex **1** was active against the DLD-1 line. Notably, complex **3** displayed approximately twice the potency of cisplatin against the 8505C cell line. It also exhibited comparable activity to cisplatin against A549 and A2780, but showed reduced efficacy against DLD-1. The water-soluble complex **2** exhibited enhanced activity toward A2780, displaying in vitro antitumor effects similar to those of cisplatin. The activity of complex **4** was reduced compared to the *cis*-complexes and cisplatin.

A comparative analysis with Pt(II) complexes bearing a PTA ligand reported by Turel et al. [17] reveals influence of monodentate cage phosphines on cytotoxic behavior. In particular, the complex [PtCl(5-chloro-7-iodo-8-hydroxyquinolinato)(PTA)] exhibited notable cytotoxicity against A375 (IC_{50} = 2.9 μM) and A549 tumor cells (IC_{50} = 4.3 μM). Similarly, the analog [PtCl(5,7-dichloro-8-hydroxyquinolinato)(PTA)] demonstrated IC_{50} values of 3.3 μM (A375) and 2.5 μM (A549), comparable (A375) or even superior to cisplatin (A549). The highest activity was observed for [PtCl(5,7-dichloro-8-hydroxy-2-methyl-quinolinato)(PTA)], showing an IC_{50} of only 1.5 μM against A549 cells. These findings align with the present study, where (di)acetylplatinum(II) complexes bearing cage phosphines such as $PASO_2$ and DAPTA exhibited moderate to high cytotoxicity in various human cancer cell lines. Taken together, these findings suggest the potential of cage phosphine–platinum(II) systems as promising candidates for further development in platinum-based chemotherapy.

3. Materials and Methods

3.1. Chemicals

All other chemicals were obtained from Aldrich or Fluka and used without further purification. The complexes $[Pt(COMe)_2H(Cl)(bpy)]$ and $[Pt_2\{(COMe)_2H\}_2(\mu\text{-}Cl)_2]$ were prepared according to research methods [51,52].

3.2. General Considerations

All reactions were performed under an Ar atmosphere using standard Schlenk techniques. Solvents were dried and distilled before use. NMR spectra (^{1}H, ^{13}C, ^{31}P) were recorded at 27 °C on Varian Gemini 299, VXR 400, and Unity 500 spectrometers. Chemical shifts are relative to solvent signals (DMSO-d$_6$ δ_H 2.50, δ_C 39.5; CD_3OD δ_H 3.31, δ_C 49.0) as internal references. H_3PO_4 (85%) was used as external reference for ^{31}P NMR spectra. Multiplets of higher order are enclosed in inverted commas or designated as multiplet (m); the following coupling constants were obtained by simulation using the PERCH-NMR software package [53]. IR spectra were recorded on a Bruker Tensor 27-IR spectrometer with a Platinum ATR unit (Bruker Optik GmbH, Ettlingen, Germany). Microanalyses were performed by the University of Halle microanalytical laboratory using a CHNS-932 (LECO) elemental analyzer (LECO Corporation, St. Joseph, M, USA).

3.3. Synthesis of Compounds

3.3.1. DAPTA (3,5-Diacetyl-1,3,7-triaza-5-phosphabicyclo[3.3.1]-nonan)

The ligand DAPTA was prepared using a conventional method [16]. Briefly, PTA (1.0 g, 6.37 mmol) was dissolved in water (13 mL) at 0 °C. Acetic anhydride (1.9 g, 19.02 mmol) was dropped stepwise into this solution. After 20 min of stirring at 0 °C, the solution was allowed to come to room temperature. After another 30 min, the solvent was removed, and the white precipitate was recrystallized from acetone. Yield: 60% (0.87 g). ^{1}H NMR (200 MHz, CD_3OD): δ 2.05/2.07 (s/s, 6H, 2 × CH_3), 3.39–3.47 (m, 1H, PCH_2N), 3.63 (d, $^{2}J_{P,H}$ = 11.3 Hz, 2H, PCH_2N), 3.93 (ddd, 1H, PCH_2N), 4.11 (d, 1H, NCH_2N), 4.43 (d, 1H, PCH_2N), 4.66 (d, 1H, NCH_2N), 5.05 (d, 1H, NCH_2N), 5.14 (d, 1H, PCH_2N), 5.73 (d, 1H, NCH_2N).

^{13}C NMR (51 MHz, CD_3OD): δ 21.5/21.7 (s/s, 2 × CH_3), 38.7 (d, $^{1}J_{P,C}$ = 27.0 Hz, PCH_2N), 43.9 (d, $^{1}J_{P,C}$ = 27.7 Hz, PCH_2N), 47.5 (d, $^{1}J_{P,C}$ = 16.0 Hz, PCH_2N), 63.0/68.5 (s/s, 2 × NCH_2N), 171.8/172.4 (s/s, 2 × *C*O). ^{31}P NMR (81 MHz, CD_3OD): δ −74.1(s).

3.3.2. Synthesis of *cis*-[Pt(COMe)$_2$(PASO$_2$)$_2$] (**1**)

A solution of [Pt(COMe)$_2$(NH_2Bn)$_2$] (200 mg, 0.40 mmol) and $PASO_2$ (170 mg, 0.80 mmol) in dichloromethane (10 mL) was stirred for 20 min, resulting in a colorless precipitate. After the addition of diethyl ether (15 mL) to complete the precipitation of complex 1, the product was filtered off, washed with diethyl ether (3 mL), and dried in a vacuum. Yield: 190 mg (70%).

$T_{dec.}$ = 148 °C. Elem. Anal. (found. (calc.), %): $C_{14}H_{26}O_6N_6P_2S_2Pt$ (695.05), C 24.49 (24.18), H 3.69 (3.77), N 11.59 (12.08), S 9.23 (9.22). ^{1}H NMR[1] (500 MHz, DMSO-d_6): δ 1.93 (s+d, $^{3}J_{Pt,H}$ = 15.9 Hz, 6H, COCH_3), 3.97 (s, 4H, H^{m},$H^{m'}$), 4.43–4.67 (m, 8H, $H^{a}/H^{a'}/H^{b}/H^{b'}$), 4.73–5.17 (m, 8H, $H_{ax.}/H_{äq.}$). ^{13}C NMR (125 MHz, DMSO-d_6): δ 44.1 (m, calc.: $^{3}J_{P,C}$ = 25.7 Hz, $^{3}J_{P,C}$ = 2.2 Hz, $^{2}J_{P,P}$ = −17.4 Hz, $COCH_3$), 49.6 ('t', calc.: $^{1}J_{P,C}$ = 11.7 Hz, $^{3}J_{P,C}$ = 8.2 Hz, $^{2}J_{P,P}$ = −17.4 Hz, $CH^{m}H^{m'}$), 50.8 ('t', calc.: $^{1}J_{P,C}$ = 9.7 Hz, $^{3}J_{P,C}$ = 6.5 Hz, $^{2}J_{P,P}$ = −17. Hz, $CH^{a/b}H^{a'/b'}$), 71.4 (s, $CH_{ax.}/H_{äq.}$), 242.4 ('dd', *C*O). ^{31}P NMR (81 MHz, DMSO-d_6): δ −77.2 (s+d, $^{1}J_{Pt,P}$ = 1440 Hz). ESI-MS: m/z (Int. found./calc. for [Pt(COMe)$_2$(PASO$_2$)$_2$Na]$^{+}$, %) 716.04 (0/2), 717.03 (80/82), 718.04 (100/100), 719.04 (81/89), 720.04 (21/24), 721.04 (25/28). IR: λ 2973 (w), 1600 (s), 1372 (s), 1336 (m), 1171 (s), 828 (s), 755 (s), 705 (s), 570 (s), 455 (s) cm^{-1}

3.3.3. Synthesis of *cis*-[Pt(COMe)$_2$(DAPTA)$_2$] (**2**)

Into a solution of [Pt(COMe)$_2$(NH_2Bn)$_2$] (250 mg, 0.51 mmol) in dichlormethane (10 mL), a solution of DAPTA (250 mg, 1.10 mmol) in dichlormethane (5 mL) was dropped slowly with stirring. After 15 min, diethyl ether (10 mL) was added. The precipitate formed

was filtered off, washed with diethyl ether (3 mL), and then dried under vacuum. Yield: 263 mg (71%). $T_{dec.}$ = 141 °C (color change: white to brown). Elem. Anal. (found. (calc.), %): $C_{22}H_{38}O_6N_6P_2Pt$ (739.60), C 35.84 (35.73), H 5.24 (5.18), N 10.90 (11.36). ^{1}H NMR (500 MHz, CD_3OD): δ 2.07/2.09 (s/s, 12H, 2 × NCOCH_3), 2.13 (s+d, $^3J_{Pt,H}$ = 17.2 Hz, 6H, PtCOCH_3), 3.53–3.66 (m, 2H, PCH_2N), 3.80 (m, 4H, PCH_2N), 4.12 (m, 4H, PCH_2N + NCH_2N), 4.55 (d, 2H, PCH_2N), 4.68 (d, 2H, NCH_2N), 5.08 (d, 2H, NCH_2N), 5.26 (m, 2H, PCH_2N), 5.70 (d, 2H, NCH_2N). ^{13}C NMR (125 MHz, CD_3OD): δ 21.4/21.8 (s/s, 2 × NCOCH_3), 40.6/45.4 (m/m, 2 × PCH_2N), 44.4 (m, PtCOCH_3 + PCH_2N), 66.9/68.1 (s/s, 2 × NCH_2N), 171.9/172.2 (s/s, 2 × NCOCH_3), 253.1 ('dd', PtCOCH_3). ^{31}P NMR (81 MHz, CD_3OD): δ −42.2 (d+dd, $^1J_{Pt,P}$ = 1496 Hz). IR: λ 3444 (w), 2930 (w), 1629 (s), 1435 (s), 1350 (s), 1236 (m), 1100 (m), 985 (m), 892 (s), 799 (s) cm^{-1}.

3.3.4. Synthesis of *trans*-[Pt(COMe)Cl($PASO_2$)] (**3**)

(a) From the reaction of complex **2** with HCl

To a suspension of **1** (100 mg, 0.14 mmol) in methanol (10 mL), diluted HCl (6%, 0.51 mL, 0.85 mmol) was added dropwise, very slowly. The reaction mixture was stirred for 18 days at room temperature. Then, diethyl ether (10 mL) was added. The precipitate was filtered off, washed with a methanolic solution of NaOMe (0.4 M, 5 mL, 2.0 mmol), then washed with diethyl ether (8 mL), and finally dried under vacuum. Yield 60 mg (70%), with 20% contamination. ^{1}H NMR (200 MHz, DMSO-d_6): δ 2.21 (s+d, $^3J_{Pt,H}$ = 12.6 Hz, 3H, COCH_3), 4.12 (s, 4H, $H^mH^{m'}$), 4.58–4.70 (m, 8H, H^a,$H^{a'}$,H^b,$H^{b'}$), 4.71–5.18 (m, 8H, $H_{eq.}$,$H_{ax.}$). ^{31}P-NMR (81 MHz, DMSO-d_6): δ −67.2 (s+d, $^1J_{Pt,P}$ = 3325 Hz).

(b) From the reaction of complex [Pt_2{$(COMe)_2H$}$_2$(μ-Cl)$_2$] with $PASO_2$

To a solution of [Pt_2{$(COMe)_2H$}$_2$(μ-Cl)$_2$] (200 mg, 0.31 mmol) in dichloromethane (10 mL), a suspension of $PASO_2$ (130 mg, 0.63 mmol) in dichloromethane (5 mL) was slowly added with stirring. After 2 h, diethyl ether (10 mL) was added. The colorless precipitate was filtered off, washed with diethyl ether (5 mL), and then dried under vacuum. Yield: 161 mg (37%). Elem. Anal. (found. (calc.), %): $C_{12}H_{23}ClO_5N_6P_2S_2Pt$ (687.95), C 21.07 (20.95), H 3.48 (3.37), N 12.19 (12.22), S 9.34 (9.32). ^{1}H NMR (200 MHz, DMSO-d_6): δ 2.22 (s, 3H, COCH_3), 4.13 (s, 4H, $H^m/H^{m'}$), 4.63–5.16 (m, 17H, $H^a/H^{a'}/H^b/H^{b'}/H_{ax.}/H_{eq.}$). ^{13}C NMR (125 MHz, DMSO-d_6): δ 48.1 (t, $^1J_{P,C}$ = 10.6 Hz, PCH^{m}H$^{m'}$N), 48.8 (m, PCH$^{a/b}$H$^{a'/b'}$N + *C*OCH$_3$), 72.1 (s, NCH$_2$N), 209.3 (t, $^2J_{P,C}$ = 5.0 Hz, $^1J_{Pt,C}$ = 848 Hz, *C*OCH$_3$). ^{31}P NMR (81 MHz, DMSO-d_6): δ −67.8 (s+d $^1J_{Pt,P}$ = 3359 Hz).

3.3.5. Synthesis of *trans*-[Pt(COMe)Cl(DAPTA)] (**4**)

At −80 °C, to a solution of [Pt_2{$(COMe)_2H$}$_2$(μ-Cl)$_2$] (150 mg, 0.24 mmol) in methanol (5 mL), DAPTA (110 mg, 0.48 mmol) was added with stirring. After 15 min of stirring at −80 °C, the solvent was removed under vacuum, and the solid residue was dissolved in dichloromethane (3 mL). The addition of diethyl ether (6 mL) resulted in the precipitation of the product, which was filtered off, washed with diethyl ether (6 mL), and dried under vacuum. Yield: 150 mg (85%). Elem. Anal. (found. (calc.), %): $C_{20}H_{35}ClO_5N_6P_2Pt$ (732.02), C 33.01 (32.82), H 4.79 (4.82), N 11.59 (11.48). ^{1}H NMR (400 MHz, DMSO-d_6): δ 1.88/1.90 (s/s, 12H, 2 × NCOCH_3), 2.31 (s, 3H, PtCOCH_3), 3.48–3.69 (m, 2H, PCH_2N), 3.85 (s, 4H, PCH_2N), 4.05–4.22 (m, 4H, PCH_2N + NCH_2N), 4.49–4.66 (m, 4H, PCH_2N + NCH_2N), 4.88–5.30 (m, 4H, PCH_2N + NCH_2N), 5.49 (d, 2H, NCH_2N). ^{31}P NMR (81 MHz, DMSO-d_6): δ −35.0 (s+d, 3200 Hz).

3.4. Theoretical Structural Analysis

Geometry optimizations of the selected structures were carried out using the Gaussian 09 software (version C.01) package (Gaussian, Inc., Wallingford, CT, USA) [54] at the B3LYP/6-311++G(d,p) level for H, C, N, O, P, and Cl atoms, combined with the LanL2DZ

basis set for Pt [55–57]. This computational approach has been previously validated for studying structural characteristics of platinum complexes, as reported in references [58,59]. All optimizations were performed without imposing any geometric constraints. To better reflect experimental conditions, solvent effects (chloroform and methanol) were included using the Conductor-Like Polarizable Continuum Model (CPCM) [60], corresponding to the solvents used for NMR measurements.

NMR chemical shifts were computed using the Gauge-Independent Atomic Orbital (GIAO) method [61,62], with tetramethylsilane (TMS) as the internal reference. Stabilizing interactions within the structures were further analyzed using the Quantum Theory of Atoms in Molecules (QTAIM) [63,64], implemented in the AIMAll program Version 19.10.12 (TK Gristmill Software, Overland Park, KS, USA). For QTAIM calculations, the input wavefunction files (.wfx) were generated using Gaussian 09.

3.5. In Vitro Cytotoxic Studies

The cell lines 518A2, 8505C, A253, MCF-7, and SW480 were generously provided by Dr. Thomas Müller from the Department of Hematology/Oncology at Martin Luther University of Halle-Wittenberg, Halle (Saale), Germany. Cells were cultured as monolayers in RPMI 1640 medium (PAA Laboratories, Pasching, Austria), supplemented with 10% fetal bovine serum (Biochrom AG, Berlin, Germany) and penicillin/streptomycin (PAA Laboratories), and maintained at 37 °C in a humidified incubator with 5% CO_2.

Stock solutions of the test compounds were freshly prepared in dimethyl sulfoxide (DMSO; Sigma-Aldrich, Darmstadt, Germany) at a concentration of 20 mM, sterilized using a 0.22 µm Millipore filter, and subsequently diluted in culture medium to the desired working concentrations. The nutrient medium used for dilution was RPMI 1640, supplemented as described above.

Cytotoxicity was assessed using the sulforhodamine B (SRB) colorimetric assay (Sigma-Aldrich, Germany), following standard protocols [65]. Cells were exposed to a range of compound concentrations (0–100 µM) for 96 h, and all treatments were conducted in triplicate. The final concentrations of DMSO in any well did not exceed 0.5%, a level shown to be non-toxic to the cells. Absorbance was measured at 570 nm using a 96-well microplate reader (Tecan Spectra, Crailsheim, Germany). Half-maximal inhibitory concentrations (IC_{50} values) were determined from semi-logarithmic dose–response curves.

4. Conclusions

Four novel acetylplatinum(II) complexes containing $PASO_2$ and DAPTA ligands were synthesized and characterized using spectroscopic and theoretical methods. The square planar coordination geometry of the Pt(II) center was confirmed for both *cis*- and *trans*-isomers based on NMR data and DFT optimization at the B3LYP/6-311++G(d,p)(C,H,N,O,P,Cl)/LanL2DZ(Pt) level of theory. Structural differences between *cis*- and *trans*-configured species were reflected in variations in bond lengths, angles, and the nature of the non-covalent interactions.

Theoretical and experimental ^{1}H and ^{13}C NMR chemical shifts of *cis*-[$Pt(COMe)_2(DAPTA)_2$] (**1**) showed strong agreement, confirming the reliability of the selected computational approach. QTAIM analysis provided further insight into bonding interactions, indicating a partially covalent character for Pt–C and Pt–P bonds in all the complexes, along with stabilizing closed-shell interactions such as H···H, O···H, and H···Cl contacts. These interactions were more prominent in the *cis*-isomers, contributing to their increased stability.

Cytotoxicity studies revealed that *cis*-[$Pt(COMe)_2(PASO_2)_2$] (**1**) displayed significant activity against the 8505C and A253 cell lines, outperforming cisplatin in the former. The DAPTA-containing complex **2** exhibited strong activity toward A2780 ovarian cancer cells.

In contrast, the *trans*-configured complex 4 demonstrated reduced overall cytotoxicity. $PASO_2$ and DAPTA alone were inactive under the tested conditions.

The integration of synthetic, spectroscopic, theoretical, and biological analyses has enabled a comprehensive evaluation of the structural and functional attributes of $PASO_2$- and DAPTA-based Pt(II) complexes, underlining the importance of ligand geometry and donor environment in modulating antitumor activity.

Supplementary Materials: The following supporting information can be downloaded at https://www.mdpi.com/article/10.3390/inorganics13080253/s1. Figure S1: ^{13}C and ^{31}P NMR spectra of **1** (DMSO-d_6, 125 and 81 MHz, respectively); Figure S2: ^{13}C and ^{31}P NMR spectra of **2** (CD_3OD, 125 and 81 MHz, respectively); Figure S3: ^{1}H, ^{13}C, and ^{31}P NMR spectra of **3** (CD_3OD, 200, 125 and 81 MHz, respectively); Figure S4: ^{1}H and ^{31}P NMR spectra of **4** (CD_3OD, 400 and 81 MHz, respectively); Figure S5: Stability of **1** over 96 h, ^{31}P NMR spectra (DMSO-d_6, 81 MHz); Optimized geometries of complexes **1–4**.

Author Contributions: Conceptualization, F.M. and G.N.K.; methodology, D.D., M.R.K., F.M. and G.N.K.; software, S.R.; validation, S.R., D.D. and M.R.K.; formal analysis, S.R.; investigation, S.R., D.D. and M.R.K.; resources, F.M. and G.N.K.; data curation, S.R.; writing—original draft preparation, S.R., D.D. and G.N.K.; writing—review and editing, S.R., D.D., M.R.K., F.M. and G.N.K.; visualization, D.D. and G.N.K.; supervision, D.D. and G.N.K.; project administration, G.N.K. All authors have read and agreed to the published version of the manuscript.

Funding: The authors acknowledge the financial support of the Ministry of Science, Technological Development and Innovation of the Republic of Serbia (Nos. 451-03-137/2025-03/200146 and 451-03-136/2025-03/200146) and by the German Academic Exchange Service (DAAD HAW EURABridge Projekt-ID: 57656312).

Institutional Review Board Statement: Not applicable.

Informed Consent Statement: Not applicable.

Data Availability Statement: The data are contained in this article. Further inquiries can be directed to the corresponding author.

Acknowledgments: We would like to thank Dirk Steinborn (Martin Luther University Halle Wittenberg, Germany) for his great help related to this project.

Conflicts of Interest: The authors declare no conflicts of interest. The funders had no role in the design of the study; in the collection, analyses, or interpretation of data; in the writing of the manuscript; or in the decision to publish the results.

References

1. Zoń, A.; Bednarek, I. Cisplatin in Ovarian Cancer Treatment—Known Limitations in Therapy Force New Solutions. *Int. J. Mol. Sci.* **2023**, *24*, 7585. [CrossRef] [PubMed]
2. Coffetti, G.; Moraschi, M.; Facchetti, G.; Rimoldi, I. The Challenging Treatment of Cisplatin-Resistant Tumors: State of the Art and Future Perspectives. *Molecules* **2023**, *28*, 3407. [CrossRef] [PubMed]
3. Kaluderovic, G.N.; Paschke, R. Anticancer Metallotherapeutics in Preclinical Development. *Curr. Med. Chem.* **2011**, *18*, 4738–4752. [CrossRef] [PubMed]
4. Abdolmaleki, S.; Khaksar, S.; Aliabadi, A.; Panjehpour, A.; Motieiyan, E.; Marabello, D.; Faraji, M.H.; Beihaghi, M. Cytotoxicity and Mechanism of Action of Metal Complexes: An Overview. *Toxicology* **2023**, *492*, 153516. [CrossRef] [PubMed]
5. Biswal, S.; Panda, M.; Sahoo, R.K.; Tripathi, S.K.; Biswal, B.K. Tumour Microenvironment and Aberrant Signaling Pathways in Cisplatin Resistance and Strategies to Overcome in Oral Cancer. *Arch. Oral Biol.* **2023**, *151*, 105697. [CrossRef] [PubMed]
6. Arjmand, F.; Khan, H.Y.; Tabassum, S. Progress of Metal-Based Anticancer Chemotherapeutic Agents in Last Two Decades and Their Comprehensive Biological (DNA/RNA Binding, Cleavage and Cytotoxicity Activity) Studies. *Chem. Rec.* **2023**, *23*, e202200247. [CrossRef] [PubMed]
7. Todorov, L.; Kostova, I. Recent Trends in the Development of Novel Metal-Based Antineoplastic Drugs. *Molecules* **2023**, *28*, 1959. [CrossRef] [PubMed]

8. Singh, A.K.; Kumar, A.; Singh, H.; Sonawane, P.; Pathak, P.; Grishina, M.; Yadav, J.P.; Verma, A.; Kumar, P. Metal Complexes in Cancer Treatment: Journey So Far. *Chem. Biodivers.* **2023**, *20*, e202300061. [CrossRef] [PubMed]
9. Predarska, I.; Saoud, M.; Morgan, I.; Lönnecke, P.; Kaluđerović, G.N.; Hey-Hawkins, E. Triphenyltin(IV) Carboxylates with Exceptionally High Cytotoxicity against Different Breast Cancer Cell Lines. *Biomolecules* **2023**, *13*, 595. [CrossRef] [PubMed]
10. Ansari, M.F.; Khan, H.Y.; Tabassum, S.; Arjmand, F. Advances in Anticancer Alkaloid-Derived Metallo-Chemotherapeutic Agents in the Last Decade: Mechanism of Action and Future Prospects. *Pharmacol. Ther.* **2023**, *241*, 108335. [CrossRef] [PubMed]
11. Schatzschneider, U. 14. Metallointercalators and Metalloinsertors: Structural Requirements for DNA Recognition and Anticancer Activity. In *Metallo-Drugs: Development and Action of Anticancer Agents*; De Gruyter: Berlin, Germany, 2018; pp. 387–436.
12. Ferraro, M.G.; Piccolo, M.; Misso, G.; Santamaria, R.; Irace, C. Bioactivity and Development of Small Non-Platinum Metal-Based Chemotherapeutics. *Pharmaceutics* **2022**, *14*, 954. [CrossRef] [PubMed]
13. Borutzki, Y.; Skos, L.; Gerner, C.; Meier-Menches, S.M. Exploring the Potential of Metal-Based Candidate Drugs as Modulators of the Cytoskeleton. *ChemBioChem* **2023**, *24*, e202300178. [CrossRef] [PubMed]
14. Guerriero, A.; Gonsalvi, L. From Traditional PTA to Novel CAP: A Comparison between Two Adamantane Cage-Type Aminophosphines. *Inorganica Chim. Acta* **2021**, *518*, 120251. [CrossRef]
15. Fisher, K.J.; Dance, I.G.; Willett, G.D.; Zhang, R.; Alyea, E.C. Electrospray Studies of a Water Soluble Platinum (II) Phosphine Complex, Chlorotris(1,3,5-Triaza-7-Phosphaadamantane)Platinum (II) Chloride $(TPA)_3PtCl_2$. *Eur. J. Mass Spectrom.* **2000**, *6*, 23–30. [CrossRef]
16. Phillips, A.D.; Gonsalvi, L.; Romerosa, A.; Vizza, F.; Peruzzini, M. Coordination Chemistry of 1,3,5-Triaza-7-Phosphaadamantane (PTA). *Coord. Chem. Rev.* **2004**, *248*, 955–993. [CrossRef]
17. Živković, M.D.; Kljun, J.; Ilic-Tomic, T.; Pavic, A.; Veselinović, A.; Manojlović, D.D.; Nikodinovic-Runic, J.; Turel, I. A New Class of Platinum(II) Complexes with the Phosphine Ligand Pta Which Show Potent Anticancer Activity. *Inorg. Chem. Front.* **2018**, *5*, 39–53. [CrossRef]
18. Smoleński, P.; Śliwińska-Hill, U.; Kwiecień, A.; Wolińska, J.; Poradowski, D. Design, Synthesis, and Anti-Cancer Evaluation of Novel Water-Soluble Copper(I) Complexes Bearing Terpyridine and PTA Ligands. *Molecules* **2024**, *29*, 945. [CrossRef] [PubMed]
19. López-Sánchez, B.; Scalambra, F.; Romerosa, A. Transformation of the Pheromone 3-methyl-2-cyclohexen-1-ol in the Presence of $[RuClCp(PTA)_2]$ and $[RuCp(OH_2)(PTA)_2]CF_3SO_3$. *Appl. Organom. Chemis.* **2024**, *38*, e7368. [CrossRef]
20. Lorenzon, T.; Vescovo, M.; Maiullari, M.; Tonon, G.; Conceição, N.R.; Carabineiro, S.A.C.; Mahmoud, A.G.; Dietl, M.C.; Demitri, N.; Orian, L.; et al. Influence of the Charge of 1,3,5-Triaza-7-Phosphaadamantane-Based Ligands on the Anticancer Activity of Organopalladium Complexes. *RSC Adv.* **2025**, *15*, 14058–14071. [CrossRef] [PubMed]
21. Braddock-Wilking, J.; Acharya, S.; Rath, N.P. Synthesis and Characterization of Pt(II) and Pd(II) PTA and DAPTA Complexes. *Polyhedron* **2014**, *79*, 16–28. [CrossRef]
22. Sheelakumari, S.P.; Cappellari, M.V.; Rivas Aiello, M.B.; Hepp, A.; Strassert, C.A. Synthesis and Photophysical Evaluation of Isoleptic Pt(II) and Pd(II) Complexes Utilizing NˆNˆN Ligands as Luminophoric Chelators with Different Ancillary Ligands. *Inorganics* **2024**, *12*, 58. [CrossRef]
23. Smoleński, P.; Mukhopadhyay, S.; Guedes Da Silva, M.F.C.; Charmier, M.A.J.; Pombeiro, A.J.L. New Water-Soluble Azido- and Derived Tetrazolato-Platinum(Ii) Complexes with PTA. Easy Metal-Mediated Synthesis and Isolation of 5-Substituted Tetrazoles. *Dalton Trans.* **2008**, 6546–6555. [CrossRef] [PubMed]
24. Guerrero, E.; Miranda, S.; Lüttenberg, S.; Fröhlich, N.; Koenen, J.-M.; Mohr, F.; Cerrada, E.; Laguna, M.; Mendía, A. *Trans* -Thionate Derivatives of Pt(II) and Pd(II) with Water-Soluble Phosphane PTA and DAPTA Ligands: Antiproliferative Activity against Human Ovarian Cancer Cell Lines. *Inorg. Chem.* **2013**, *52*, 6635–6647. [CrossRef] [PubMed]
25. Mohr, F.; Cerrada, E.; Laguna, M. Organometallic Gold(I) and Gold(III) Complexes Containing 1,3,5-Triaza-7-Phosphaadamantane (TPA): Examples of Water-Soluble Organometallic Gold Compounds. *Organometallics* **2006**, *25*, 644–648. [CrossRef]
26. Mohr, F.; Sanz, S.; Tiekink, E.R.T.; Laguna, M. Water-Soluble and Water-Stable Organometallic Gold(II) Complexes. *Organometallics* **2006**, *25*, 3084–3087. [CrossRef]
27. Darensbourg, D.J.; Yarbrough, J.C.; Lewis, S.J. 2-Thia-1,3,5-Triaza-7-Phosphaadamantane 2,2-Dioxide $(PASO_2)$. Comparative Structural and Reactivity Investigation with the Water-Soluble Phosphine Ligand 1,3,5-Triaza-7-Phosphaadamantane (PTA). *Organometallics* **2003**, *22*, 2050–2056. [CrossRef]
28. Mahmoud, A.; Smoleński, P.; Guedes Da Silva, M.; Pombeiro, A. Water-Soluble O-, S- and Se-Functionalized Cyclic Acetyl-Triaza-Phosphines. Synthesis, Characterization and Application in Catalytic Azide-Alkyne Cycloaddition. *Molecules* **2020**, *25*, 5479. [CrossRef] [PubMed]
29. Gosavi, T.; Rusanov, E.; Schmidt, H.; Steinborn, D. Reactivity of Platina-β-Diketones towards Chelating Nitrogen and Sulfur Donors: Formation of Acyl(Hydrido)Platinum(IV) and Acyl(Chloro)Platinum(II) Complexes. *Inorganica Chim. Acta* **2004**, *357*, 1781–1788. [CrossRef]

30. Kluge, T.; Mendicute-Fierro, C.; Bette, M.; Rodríguez-Diéguez, A.; Garralda, M.A.; Steinborn, D. On the Reactivity of Platina-β-diketone and Acetylplatinum(II) Complexes toward 2-(Diphenylphosphanyl)Benzaldehyde and Its Dioxolane Derivative. *Eur. J. Inorg. Chem.* **2013**, *2013*, 5418–5427. [CrossRef]
31. Albrecht, C.; Wagner, C.; Steinborn, D. Zur Reaktivität von Dinuklearen Platina-β-Diketonen Gegenüber Phosphanen: Diacetylplatin(II)-Komplexe Und Mononukleare Platina-β-Diketone. *Z. Anorg. Allg. Chem.* **2008**, *634*, 2858–2866. [CrossRef]
32. Albrecht, C. Synthese und Charakterisierung Neuartiger Platinkomplexe und -Cluster. Ph.D. Dissertation, Martin-Luther-Universität Halle-Wittenberg, Halle, Germany, 2007.
33. Hesse, M.; Meier, H.; Zeeh, B. *Spektroskopische Methoden in Der Organischen Chemie*, 7th ed.; Georg Thieme Verlag: Stuttgart, Germany, 2002.
34. Steinborn, D.; Hoffmann, T.; Gerisch, M.; Bruhn, C.; Schmidt, H.; Nordhoff, K.; Davies, J.A.; Kirschbaum, K.; Jolk, I. On the Reactivity of Platina-β-Diketones—Synthesis and Characterization of Acylplatinum(II) Complexes. *Z. Anorg. Allg. Chem.* **2000**, *626*, 661–666. [CrossRef]
35. Bippus, P.; Skocic, M.; Jakupec, M.A.; Keppler, B.K.; Mohr, F. Synthesis, Structures and In Vitro Cytotoxicity of Some Cationic Cis-Platinum(II) Complexes Containing Chelating Thiocarbamates. *J. Inorg. Biochem.* **2011**, *105*, 462–466. [CrossRef] [PubMed]
36. Hall, M.D.; Telma, K.A.; Chang, K.-E.; Lee, T.D.; Madigan, J.P.; Lloyd, J.R.; Goldlust, I.S.; Hoeschele, J.D.; Gottesman, M.M. Say No to DMSO: Dimethylsulfoxide Inactivates Cisplatin, Carboplatin, and Other Platinum Complexes. *Cancer Res.* **2014**, *74*, 3913–3922. [CrossRef] [PubMed]
37. Yousef, R.I.; Bette, M.; Kaluđerović, G.N.; Paschke, R.; Yiran, C.; Steinborn, D.; Schmidt, H. Structure Determination and Investigation on Cytotoxicity of Potassium Dichlorido(l-Prolinato)Platinate(II) versus Chlorido(Dimethyl Sulfoxide)(l-Prolinato)Platinum(II) Complex—In Vitro Antitumor Deactivation by Cl−/Dmso Ligand Exchange. *Polyhedron* **2011**, *30*, 1990–1996. [CrossRef]
38. Moto Ongagna, J.; Tamafo Fouegue, A.D.; Ateba Amana, B.; Mouzong D'ambassa, G.; Zobo Mfomo, J.; Mbaze Meva'A, L.; Bikele Mama, D. B3LYP, M06 and B3PW91 DFT Assignment of Nd8 Metal-Bis-(N-Heterocyclic Carbene) Complexes. *J. Mol. Model* **2020**, *26*, 246. [CrossRef] [PubMed]
39. Yılmaz, İ.; Acar-Selçuki, N.; Coles, S.J.; Pekdemir, F.; Şengül, A. Spectroscopic, Structural and DFT Studies of Luminescent Pt(II) and Ag(I) Complexes with an Asymmetric 2,2′-Bipyridine Chelating Ligand. *J. Mol. Struct.* **2021**, *1223*, 129271. [CrossRef]
40. Carpenter, J.P.; Lukehart, C.M. Probing the Electronic Structure of Selected Diplatinum (μ-Alkenylidene) Complexes. *Inorganica Chim. Acta* **1991**, *190*, 7–10. [CrossRef]
41. Cohen, R.D.; Wood, J.S.; Lam, Y.-H.; Buevich, A.V.; Sherer, E.C.; Reibarkh, M.; Williamson, R.T.; Martin, G.E. DELTA50: A Highly Accurate Database of Experimental 1H and 13C NMR Chemical Shifts Applied to DFT Benchmarking. *Molecules* **2023**, *28*, 2449. [CrossRef] [PubMed]
42. Pankratyev, E.Y.; Tulyabaev, A.R.; Khalilov, L.M. How Reliable Are GIAO Calculations of ^{1}H and ^{13}C NMR Chemical Shifts? A Statistical Analysis and Empirical Corrections at DFT (PBE/3z) Level. *J. Comput. Chem.* **2011**, *32*, 1993–1997. [CrossRef] [PubMed]
43. Kasalović, M.P.; Dimić, D.; Jelača, S.; Maksimović-Ivanić, D.; Mijatović, S.; Zmejkovski, B.B.; Schreiner, S.H.F.; Rüffer, T.; Pantelić, N.; Kaluđerović, G.N. Trimethyltin(IV) Bearing 3-(4-Methyl-2-Oxoquinolin-1(2H)-Yl)Propanoate Causes Lipid Peroxidation-Mediated Autophagic Cell Death in Human Melanoma A375 Cells. *Pharmaceuticals* **2024**, *17*, 372. [CrossRef] [PubMed]
44. Li, Y.; Zhang, G.; Chen, D. Theoretical Investigation of Hydrogen Bonding between Water and Platinum(II): An Atom in Molecule (AIM) Study. *Mol. Phys.* **2012**, *110*, 179–184. [CrossRef]
45. Kasalović, M.P.; Jelača, S.; Milanović, Ž.; Maksimović-Ivanić, D.; Mijatović, S.; Lađarević, J.; Božić, B.; Marković, Z.; Dunđerović, D.; Rüffer, T.; et al. Novel Triphenyltin(iv) Compounds with Carboxylato *N*-Functionalized 2-Quinolones as Promising Potential Anticancer Drug Candidates: In Vitro and In Vivo Evaluation. *Dalton Trans.* **2024**, *53*, 8298–8314. [CrossRef] [PubMed]
46. Soliman, S.M.; Albering, J.; Abu-Youssef, M.A.M. Structural Analyses of Two New Highly Distorted Octahedral Copper(II) Complexes with Quinoline-Type Ligands; Hirshfeld, AIM and NBO Studies. *Polyhedron* **2017**, *127*, 36–50. [CrossRef]
47. Lepetit, C.; Vabre, B.; Canac, Y.; Alikhani, M.E.; Zargarian, D. Pentacoordinated, Square Pyramidal Cationic PCP Ni(II) Pincer Complexes: ELF and QTAIM Topological Analyses of Nickel–Triflate Interactions. *Theor. Chem. Acc.* **2018**, *137*, 141. [CrossRef]
48. Bianchi, R.; Gervasio, G.; Marabello, D. Experimental Electron Density Analysis of Mn 2 (CO) 10: Metal−Metal and Metal−Ligand Bond Characterization. *Inorg. Chem.* **2000**, *39*, 2360–2366. [CrossRef] [PubMed]
49. Espinosa, E.; Molins, E.; Lecomte, C. Hydrogen Bond Strengths Revealed by Topological Analyses of Experimentally Observed Electron Densities. *Chem. Phys. Lett.* **1998**, *285*, 170–173. [CrossRef]
50. Szmigiel-Bakalarz, K.; Nentwig, M.; Oeckler, O.; Malik-Gajewska, M.; Filip-Psurska, B.; Morzyk-Ociepa, B. 7-Azaindole-3-Carboxylic Acid and Its Pt(II) and Pd(II) Complexes: Crystal Structure of the Ligand, Vibrational Spectra, DFT Calculations and In Vitro Antiproliferative Activity. *J. Mol. Struct.* **2020**, *1203*, 127441. [CrossRef]
51. Werner, M.; Bruhn, C.; Steinborn, D. From Platina-β-Diketones to Diacetylplatinum(II) Complexes—Synthesis, Characterization and Structural Features. *J. Organomet. Chem.* **2008**, *693*, 2369–2376. [CrossRef]

52. Gerisch, M.; Heinemann, F.W.; Bruhn, C.; Scholz, J.; Steinborn, D. Reactivity of Dinuclear Platina-β-Diketones toward Phosphines and Pyridines: Formation of Mononuclear Platina-β-Diketones and Acyl(Chloro)Platinum(II) Complexes. *Organometallics* **1999**, *18*, 564–572. [CrossRef]
53. Renfrew, A.K.; Phillips, A.D.; Egger, A.E.; Hartinger, C.G.; Bosquain, S.S.; Nazarov, A.A.; Keppler, B.K.; Gonsalvi, L.; Peruzzini, M.; Dyson, P.J. Influence of Structural Variation on the Anticancer Activity of RAPTA-Type Complexes: Ptn versus Pta. *Organometallics* **2009**, *28*, 1165–1172. [CrossRef]
54. Frisch, M.J.; Trucks, G.W.; Schlegel, H.B.; Scuseria, G.E.; Robb, M.A.; Cheeseman, J.R.; Scalmani, G.; Barone, V.; Mennucci, B.; Petersson, G.A.; et al. *Gaussian 09*; Gaussian, Inc.: Wallingford, CT, USA, 2009.
55. Becke, A.D. Density-Functional Thermochemistry. III. The Role of Exact Exchange. *J. Chem. Phys.* **1993**, *98*, 5648. [CrossRef]
56. Dunning, T.H. Gaussian Basis Sets for Use in Correlated Molecular Calculations. I. The Atoms Boron through Neon and Hydrogen. *J. Chem. Phys.* **1989**, *90*, 1007. [CrossRef]
57. Wadt, W.R.; Hay, P.J. *Ab Initio* Effective Core Potentials for Molecular Calculations. Potentials for Main Group Elements Na to Bi. *J. Chem. Phys.* **1985**, *82*, 284–298. [CrossRef]
58. Mohamed, D.S.; Al-Jibori, S.A.; Behjatmanesh-Ardakani, R.; Faihan, A.S.; Yousef, T.A.; Alhamzani, A.G.; Abou-Krisha, M.M.; Al-Janabi, A.S.M.; Hsiao, B.S. Spectroscopic, Anti-Cancer Activity, and DFT Computational Studies of Pt(II) Complexes with 1-Benzyl-3-Phenylthiourea and Phosphine/Diamine Ligands. *Inorganics* **2023**, *11*, 125. [CrossRef]
59. Sankarganesh, M.; Solomon, R.V.; Raja, J.D. Platinum Complex with Pyrimidine- and Morpholine-Based Ligand: Synthesis, Spectroscopic, DFT, TDDFT, Catalytic Reduction, In Vitro Anticancer, Antioxidant, Antimicrobial, DNA Binding and Molecular Modeling Studies. *J. Biomol. Struct. Dyn.* **2021**, *39*, 1055–1067. [CrossRef] [PubMed]
60. Marenich, A.V.; Cramer, C.J.; Truhlar, D.G. Universal Solvation Model Based on Solute Electron Density and on a Continuum Model of the Solvent Defined by the Bulk Dielectric Constant and Atomic Surface Tensions. *J. Phys. Chem. B* **2009**, *113*, 6378–6396. [CrossRef] [PubMed]
61. Wolinski, K.; Hinton, J.F.; Pulay, P. Efficient Implementation of the Gauge-Independent Atomic Orbital Method for NMR Chemical Shift Calculations. *J. Am. Chem. Soc.* **1990**, *112*, 8251–8260. [CrossRef]
62. Ditchfield, R. Self-Consistent Perturbation Theory of Diamagnetism. *Mol. Phys.* **1974**, *27*, 789–807. [CrossRef]
63. Bader, R.F.W. Atoms in Molecules. *Acc. Chem. Res.* **1985**, *18*, 9–15. [CrossRef]
64. Bader, R.F.W.; Slee, T.S.; Cremer, D.; Kraka, E. Description of Conjugation and Hyperconjugation in Terms of Electron Distributions. *J. Am. Chem. Soc.* **1983**, *105*, 5061–5068. [CrossRef]
65. Demakova, M.Y.; Luzyanin, K.V.; Starova, G.L.; Kukushkin, V.Y. Facile Alternative Route to Cis -[PtCl 2 (PTA) 2] and [PtCl(PTA) 3]Cl (PTA = 1,3,5-Triaza-7-Phosphaadamantane). *Inorg. Chem. Commun.* **2014**, *50*, 17–18. [CrossRef]